

1 Notice

2 An edited version of this paper was published by AGU. Copyright (2020)
3 American Geophysical Union. The citation for this paper is

4 Kim, J. E., Laguë, M. M., Pennypacker, S., Dawson, E., & Swann, A. L. S.
5 (2020). Evaporative resistance is of equal importance as surface Albedo in
6 high-latitude surface temperatures due to cloud feedbacks. *Geophysical Re-*
7 *search Letters*, 47. e2019GL085663 <https://doi.org/10.1029/2019GL085663>

8 To view the published open abstract, go to <http://dx.doi.org> and enter the
9 DOI or the "Peer-reviewed Publication DOI" link will be on the right hand
10 side of this webpage.

11 **Evaporative Resistance is of Equal Importance as**
12 **Surface Albedo in High Latitude Surface Temperatures**
13 **Due to Cloud Feedbacks**

14 **Jinhyuk E. Kim¹, Marysa M. Laguë^{1,2}, Sam Pennypacker¹, Eliza Dawson^{1,3},**
15 **Abigail L.S. Swann^{1,4}**

16 ¹Department of Atmospheric Sciences, University of Washington, Seattle, WA 98195, USA

17 ²Now at Department of Earth and Planetary Science, University of California Berkeley, Berkeley, CA
18 94709, USA

19 ³Now at School of Earth, Energy, and Environmental Sciences, Stanford University, Stanford, CA 94305,
20 USA

21 ⁴Department of Biology, University of Washington, Seattle, WA 98195, USA

22 **Key Points:**

- 23 • Two Arctic plant types with different properties cause substantial changes to land
24 surface temperature through different physical pathways
- 25 • Reducing land surface evaporative resistance increases low clouds and increases
26 shortwave cloud forcing
- 27 • Albedo directly warms the land surface, while changes in evaporation warms mostly
28 by modifying cloud cover

Corresponding author: Abigail Swann, aswann@uw.edu

Corresponding author: Jinhyuk Kim, jinhyukekim@gmail.com

Abstract

Arctic vegetation is known to influence Arctic surface temperatures through albedo. However, it is less clear how plant evaporative resistance and albedo independently influence surface climate at high latitudes. We use surface properties derived from two common Arctic tree types to simulate the climate response to a change in land surface albedo and evaporative resistance in factorial combinations. We find that lower evaporative resistances lead to an increase of low clouds. The reflection of light due to the difference in albedos between vegetation types is similar to the loss of incident sunlight due to increased cloud cover resulting from lower evaporative resistance from vegetation change. Our results demonstrate that realistic changes in evaporative resistance can have an equal impact on surface temperature to changes in albedo, and that cloud feedbacks play a first order role in determining the surface climate response to changes in Arctic land cover.

Plain Language Summary

In the Arctic, darker land surfaces lead to warmer temperatures because they absorb more sunlight. However, there are multiple types of plants that grow in the Arctic, which differ not only in how dark they are but also how easily they release water. We investigate how different Arctic plants' absorption of sunlight and ability to release water to the atmosphere can affect temperature over Arctic land using an Earth System Model. We find that dark trees are capable of absorbing a greater fraction of the incoming sunlight than their brighter counterparts, which tends to warm the surface. In comparison, when the land surface has a harder time releasing water into the atmosphere, a smaller fraction of energy at the land surface is used to evaporate water. This warms the air above the surface, which leads to evaporation of cloud droplets and less cloud cover. As a result, more sunlight is able to reach the surface, and land surface temperatures are warmer even when the surface is relatively bright. In combination, we find that the darkness of the surface and the plants' ability to release water have an equal influence on surface temperatures over land in the Arctic.

1 Introduction

As the concentrations of atmospheric CO₂ and other greenhouse gases rise, global temperatures will continue to increase, with even larger increases at high latitudes (Collins et al., 2013). We expect that higher Arctic temperatures will lead to a poleward expansion of the tree-line (Gallimore et al., 2005; Lloyd, 2005; Jeong et al., 2011; Falloon et al., 2012). Tree-line expansion has already been observed in Alaska (Rupp et al., 2000; Lloyd, 2005) and in Sweden (Rundqvist et al., 2011). With continued warming, simulations of future climate scenarios suggest an increase in shrubs and needleleaf trees in the Arctic (Jeong et al., 2011; Falloon et al., 2012).

In addition to the current and future poleward expansion of trees at high northern latitudes, there is evidence from paleo records of expanded forest cover during past warm periods. Climate model simulations set with Mid-Holocene conditions show an expansion of boreal forest into the tundra relative to preindustrial-like conditions (Gallimore et al., 2005). There is also observational evidence for forests in the Arctic in the Late Cretaceous up to the Paleocene with deciduous trees occupying the land above 65°N (Wolfe & Upchurch, 1987; Royer et al., 2006). Along with the increased northward extent of these prehistoric forests, there are indications that these forests were deciduous, rather than the high-latitude needleleaf forests of the present day (G. Bonan, 2015).

Boreal forest communities are comprised of both needleleaf evergreen and broadleaf deciduous tree types (G. B. Bonan et al., 1992). Needleleaf trees have dark leaves (low albedo) and low transpiration rates (Chapin et al., 2000). They comprise the later suc-

77 cessional stages of the ecosystem and are characterized by slow growth rates (Van Cleve
78 et al., 1996). By contrast, deciduous broadleaf trees in Boreal forests are relatively bright
79 (higher albedo) with higher transpiration rates (Chapin et al., 2000). They grow back
80 quickly following disturbance and can dominate the ecosystem following a stand-replacing
81 disturbance event for a few hundred years (Van Cleve et al., 1996; Rupp et al., 2000),
82 with consequences for surface energy partitioning (Liu et al., 2005). Although needle-
83 leaf trees are conceptualized as, and often are, the dominant species in the ecosystem,
84 pollen records suggest that boreal forests in Alaska were dominated by deciduous broadleaf
85 vegetation following the last ice age (Edwards et al., 2005). Simulations suggest this could
86 occur again in the next century as fire frequency and intensity increases and shifts ecosys-
87 tems towards early successional plant types (Rupp et al., 2000).

88 Vegetation plays a large role in setting the terrestrial surface climate in the Arctic
89 by altering the surface energy budget through the exchanges of mass and energy be-
90 tween the land and the atmosphere. It is thought that the conversion of tundra to forests
91 in the Arctic will contribute substantially to high-latitude warming trends due to a de-
92 crease in albedo (Chapin et al., 2005), particularly as dark trees cover bright snow. Given
93 that vegetation is expected to move poleward during warmer climates, we expect this
94 migration to have a positive feedback on surface temperatures through the effect of albedo.

95 Observations and simulations of an expansion of Arctic trees suggest that warmer
96 temperatures at high latitudes have been driven primarily by the impact of a darker sur-
97 face (G. B. Bonan et al., 1992; Thomas & Rowntree, 1992; Foley et al., 1994; Chapin et
98 al., 2005; G. B. Bonan, 2008; Falloon et al., 2012; Collins et al., 2013; Chae et al., 2015).
99 However, vegetation in the Arctic can also influence the surface energy budget through
100 the flux of water to the atmosphere. The magnitude of transpiration can vary substan-
101 tially across vegetation types – in particular needleleaf evergreen trees have less evap-
102 otranspiration than leafed-out deciduous broadleaf trees in the Arctic (Chapin et al., 2000).

103 In general, the effect of variations in plant type traits other than albedo, such as
104 evaporative resistance (the difficulty for the plant to release water), on surface climate
105 in the Arctic has been less well explored. Climate model simulations of an expansion of
106 deciduous broadleaf trees (rather than needleleaf evergreen trees) at high latitudes found
107 approximately equal amounts of warming from two distinct physical processes (Swann
108 et al., 2010). The warming comes from both the change in albedo and the change in the
109 greenhouse effect from elevated water vapor concentrations due to higher water flux to
110 the atmosphere from the deciduous broadleaf trees, along with feedbacks from ocean and
111 sea-ice (Swann et al., 2010). Other studies have focused on surface roughness and found
112 that a change in vegetation from grasses and shrubs to needleleaf evergreen trees increases
113 temperature due to the change in roughness which induces a cloud feedback (Cho et al.,
114 2018), but they do not explore the changes in evaporative resistance, which we believe
115 to be an important factor to influencing the Arctic climate (Swann et al., 2010; Laguë
116 et al., 2019)

117 Swann et al. (2010) demonstrate that trees with different transpiration rates can
118 have a significant influence on the Arctic climate, however it remains unclear what the
119 independent relative contributions to Arctic climate are from albedo and transpiration.
120 With the realistic possibility that tree-line will continue to move poleward as climate warms
121 and that the forest composition may change to more deciduous broadleaf trees due to
122 an increase of fire frequency and intensity (Rupp et al., 2000; G. B. Bonan, 2008) and
123 as indicated by past climates, we need to understand how these changing properties from
124 one plant species to another can affect the Arctic climate. In this paper we address the
125 question of how albedo and resistance to surface evapotranspiration influence surface cli-
126 mate in the Arctic.

2 Methods

2.1 Model Description

For this study we use climate model simulations with an idealized representation of the land surface to quantify the atmospheric and surface climate response to changes in albedo and evaporative resistance of the vegetation individually. We used the Simple Land Interface Model (SLIM; (Laguë et al., 2019)), which replaces the Community Land Model (CLM) within the Community Earth System Model (CESM; (Hurrell et al., 2013)). SLIM has a number of user controlled prescribed surface properties, including surface albedo and surface evaporative resistance akin to a bulk canopy resistance (see Supplementary Information for more detail) making it useful for independently modifying surface properties in order to analyze the effects of a change in a single surface property. This is in contrast to a complex land surface model such as CLM, where a change in vegetation results in simultaneous changes to many surface properties. For example, we can specify the snow-free surface albedo directly in SLIM, while in CLM the surface albedo is an emergent property of flat leaf albedo values, leaf area, etc.. SLIM conserves energy, and evaluates the surface energy budget at each time step to determine a new surface temperature, soil temperature profile, and net fluxes of shortwave radiation, long-wave radiation, sensible heat, and latent heat. Through CESM, SLIM is then coupled with the Community Atmosphere Model v. 5 (CAM5; (Neale et al., 2012)), a slab ocean model ((Neale et al., 2012)), and an interactive sea ice model (CICE; (Hunke et al., 2017)). We run our simulations globally at a resolution of 1.9° latitude by 2.5° longitude.

It is important to note that there is substantial disagreement between different land models for the robustness of biophysical climate responses to vegetation change (De Noblet-Ducoudré et al., 2012). While land surface models generally agree with each other, as well as with observations, on the effects of vegetation change on radiative fluxes, there is a much larger disagreement on how vegetation change should impact the partitioning of turbulent energy into sensible and latent heat fluxes (Duveiller et al., 2018; De Noblet-Ducoudré et al., 2012). In addition, atmospheric responses to vegetation change are substantial (Laguë et al., 2019), which means that models have a large uncertainty in the impact of vegetation change on near surface climate not only from differences in the land models and their flux representations, but also in the sensitivity of various atmospheric models to changes in land surface fluxes. Both factors (bias in turbulent fluxes and atmospheric responses) contribute to substantial differences in near-surface air temperature over land (Ma et al., 2018).

2.2 Simulations

In our simulations we set the land surface in the Arctic (north of 60°N) to have uniform prescribed values for evaporative resistance and snow-free albedo corresponding to two plant types: evergreen needleleaf and deciduous broadleaf trees. We chose representative values for the albedo and evaporative resistance for each tree type by estimating them from grid cells dominated by our two plant types in a coupled land-atmosphere simulation using CLM. Needleleaf trees have a lower albedo and a higher evaporative resistance relative to broadleaf trees (Table S1). Albedo values are specified for four streams of radiation (visible direct light, visible diffuse light, near infrared direct light, near infrared diffuse light). Our idealized land model configuration allows us to independently change a single surface property, and therefore run simulations with a factorial combination of different values for albedo and evaporative resistance. For two of our four simulations, we have the plant type traits set to replicate needleleaf and broadleaf trees - that is, one simulation has needleleaf values for both albedo and evaporative resistance, while the other has broadleaf values for both properties (Fig. S1). The two additional simulations have ‘hybrid’ plant types with the albedo of one tree type paired with the evaporative resistance of the other, resulting in a brighter needleleaf tree and a darker

178 broadleaf tree. For simplicity we will refer to our four simulations as “Needleleaf” and
 179 “Broadleaf”, for tree types with the observed combinations of albedo and resistance, and
 180 “Bright Needleleaf”, and “Dark Broadleaf” for our hybrid tree types. The surface prop-
 181 erties (albedo and evaporative resistance) are applied uniformly across all non-glaciated
 182 land areas north of 60°N. That is, we effectively impose a mono-culture of each tree type
 183 across the entire Arctic region in each simulation, regardless of the present-day vegeta-
 184 tion type at each Arctic land location. Outside of the Arctic, surface properties reflect
 185 those of the present-day vegetation growing in each location and are identical in all sim-
 186 ulations.

187 We use summertime values derived from a CLM simulation where we take the June-
 188 July-August surface properties in the Northern Hemisphere and the December-January-
 189 February surface properties in the Southern Hemisphere. We choose summertime in or-
 190 der to capture snow-free albedo values and growing season resistance values. The aero-
 191 dynamic roughness of the land surface, which modulates the exchange of turbulent en-
 192 ergy (sensible and latent heat) between the land and the atmosphere, is parametrized
 193 as a function of vegetation height and is held fixed in time (varies spatially) in all sim-
 194 ulations. SLIM contains a simple snow model which allows for the prescribed bare-ground
 195 albedo to be masked by snow. Atmospheric CO₂ concentrations are set to a constant
 196 value of 367 ppm.

197 We run our simulations for 50 years, using the last 30 years for analysis and omit-
 198 ting the first 20 years to account for spin-up (see Supporting Information, Fig. S2).

199 2.3 Analysis

200 We focus our analysis on the summer months of June, July, and August, as these
 201 months have the least amount of snow cover, thus allowing us to observe the impact of
 202 the actual snow-free surface properties on the coupled climate system. Results are pre-
 203 sented as area-weighted averages for all Arctic land surfaces (regions north of 60°N) un-
 204 less otherwise noted. We report ranges of values of one standard deviation of variabil-
 205 ity in time. Significance is calculated using a student’s t-test and indicated by stippling.
 206 To account for lagged autocorrelation of up to two years, we assume $N/2=15$ degrees of
 207 freedom for the $N=30$ -year period; we find this to be a conservative estimate of the ac-
 208 tual degrees of freedom in the model using methods from Bretherton et al. (1999) (see
 209 Supporting Information, Fig. S3, S4). A p-value of 0.05 or less indicates a significant dif-
 210 ference with 95% confidence. Given that we have four experiments but no explicit ‘con-
 211 trol’ run in the classic sense, we have in some cases compared three of the experiments
 212 to a baseline of the Needleleaf tree type simulation (needleleaf albedo and needleleaf evap-
 213 orative resistance), in order to see how the runs compared to one another.

214 To illustrate if changes in moisture or temperature are causing cloud responses we
 215 use relative humidity as a proxy for cloudiness and analyze the differences in the verti-
 216 cal profile of relative humidity between simulations. We partition the contribution into
 217 two parts, one from differences in temperature (T), and another from differences in spe-
 218 cific humidity (q). We report the change in the contribution of each term relative to the
 219 normal Needleleaf run as follows:

$$\Delta RH_T = \frac{q_{ctrl}}{qsat_{exp}} - \frac{q_{ctrl}}{qsat_{ctrl}} \quad (1)$$

$$\Delta RH_q = \frac{q_{exp}}{qsat_{ctrl}} - \frac{q_{ctrl}}{qsat_{ctrl}} \quad (2)$$

220 where q_{ctrl} and $qsat_{ctrl}$ are the specific humidity and saturated specific humidity
 221 of the normal Needleleaf run and the q_{exp} and $qsat_{exp}$ are the specific humidity and sat-
 222 urated specific humidity of the other simulations that we are comparing to the normal

223 Needleleaf run. Equation 1 estimates the magnitude and sign of the change in the rel-
 224 ative humidity profile between the simulations given the change in atmospheric temper-
 225 ature alone and Equation 2 estimates the impact given the changing specific humidity
 226 alone. The total change in relative humidity compared to the normal Needleleaf exper-
 227 iment also includes a small contribution from the sensitivity of actual specific humidity
 228 to temperature in the simulations. However, we are primarily focused on the dominant,
 229 independent effects of temperature and specific humidity on the relative humidity pro-
 230 files in response to changing surface properties described by Equations 1 and 2 (Fig. S5).

231 **3 Results & Discussion**

232 Based on prior literature, we expect that higher albedo surfaces (i.e the Broadleaf
 233 and the Bright Needleleaf) will have cooler temperatures compared to lower albedo sur-
 234 faces because they should absorb a smaller fraction of shortwave radiation. This assump-
 235 tion held true for some, but not all of our simulations. The near surface air temperatures
 236 are $\sim 2^\circ\text{C}$ cooler for the Broadleaf simulation compared to the Needleleaf (Fig. 1a). How-
 237 ever, both the Bright Needleleaf and Dark Broadleaf simulations were $\sim 1^\circ\text{C}$ cooler than
 238 the normal Needleleaf simulation despite having different surface albedos (Fig. 1a). This
 239 suggests that additional processes are altering the surface energy budget beyond only
 240 the change in surface albedo.

241 **3.1 Surface Energy Budget**

242 The surface energy budget is comprised of five terms which must balance – absorbed
 243 shortwave (SW) radiation, net long wave radiation, sensible heat flux, latent heat flux,
 244 and heat storage in the ground. Averaged over the summer months, the total heat stor-
 245 age in the ground is comparable across all simulations and will not be part of the anal-
 246 ysis from here on. We find that absorbed SW radiation has a similar pattern to surface
 247 temperature across experiments (Fig. 1a,b, 2a-c, g-i). Although the albedo directly af-
 248 fects the fraction of the incident SW radiation that the surface absorbs, the simulations
 249 with the same albedos (Needleleaf & Dark Broadleaf, Bright Needleleaf & Broadleaf)
 250 differ from one another in absorbed SW radiation by $\sim 10\text{Wm}^{-2}$ – a result that can-
 251 not be explained by changes in albedo alone (Fig. 1b). Since this difference in absorbed
 252 shortwave radiation is not due to any variation in surface albedo, it must instead be the
 253 result of changes in the amount of solar radiation reaching the surface.

254 The incident shortwave radiation at the surface varies substantially between the
 255 experiments with low evaporative resistance (Broadleaf and Dark Broadleaf) and the ex-
 256 periments with high evaporative resistance (Needleleaf and Bright Needleleaf)(Fig. 1c,
 257 S6d-f). The difference of incident shortwave radiation between high and low evapora-
 258 tive resistance experiments suggests that surface evaporative resistance is altering down-
 259 welling SW radiation.

260 The absorbed shortwave and incident SW results (Fig. 1b,c) indicate that clouds
 261 are playing a first order role in feeding back on the surface energy budget in response
 262 to changes in Arctic evaporative resistance. Incident SW radiation is very similar be-
 263 tween simulations that have the same evaporative resistance but different surface albedo,
 264 suggesting that evaporative resistance is the dominant factor modifying incoming SW
 265 through cloud cover. Despite substantial differences in incoming SW radiation between
 266 the Dark Broadleaf and Bright Needleleaf simulations, they have a similar amount of SW
 267 radiation absorbed by the surface (Fig. 1b) and a similar change in surface temperature
 268 (Fig. 1a). This is because the darker surfaces in the Dark Broadleaf simulation absorb
 269 a larger fraction of the incident SW radiation than the Bright Needleleaf simulation (Fig.
 270 1b,c), while the Bright Needleleaf simulation has a larger amount of incoming SW ra-
 271 diation due to less low cloud cover resulting from the high evaporative resistance of the
 272 land surface (Fig. 1b, 2g-i). The strong impact of changing low cloud cover on the sur-

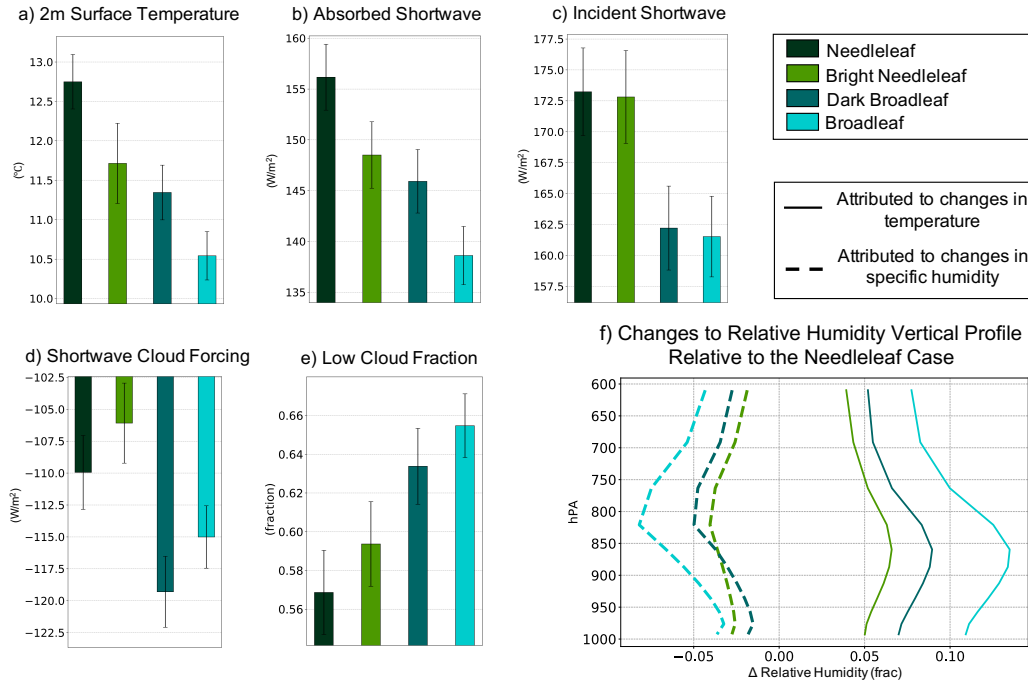


Figure 1. Arctic average fluxes, states, and cloud changes. Summertime averages over non-glaciated land North of $60^{\circ}N$ for each of four different simulations (Needleleaf, Bright Needleleaf, Dark Broadleaf, Broadleaf) for a) 2m surface temperature (C), b) absorbed shortwave radiation at the surface (Wm^{-2}), c) incident shortwave radiation at the surface (Wm^{-2}), d) shortwave cloud forcing (Wm^{-2}) with negative values indicating more clouds, and e) low cloud fraction. The error bars represent one standard deviation of variability in time. Panel f) shows changes in the relative humidity vertical profile relative to the Needleleaf case attributed to changes in the vertical profile of atmospheric temperature (solid lines) and specific humidity (dashed lines).

273 face energy budget in our simulations is consistent with observations from the Surface
 274 Heat Budget of the Arctic (SHEBA) program and at the North Slope of Alaska Atmo-
 275 spheric Radiation Measurement (ARM) site, where they show that low clouds provide
 276 a net cooling in the summer through shading (Schweiger & Key, 1994; Shupe & Intrieri,
 277 2004; Verlinde et al., 2016).

278 We expect simulations with lower evaporative resistances and higher amounts of
 279 total absorbed radiation (absorbed SW plus downwelling longwave) to have higher la-
 280 tent heat fluxes than simulations with high evaporative resistances and less total absorbed
 281 radiation. In our simulations we see that the latent heat flux is largest ($\sim 47Wm^{-2}$)
 282 for the Dark Broadleaf case, which has a high total absorbed radiation ($\sim 475Wm^{-2}$)
 283 and a low resistance to evaporation (Fig. S7a). The Bright Needleleaf simulation has a
 284 similar magnitude of total incoming radiation compared to the Dark Broadleaf simula-
 285 tion, but the resistance to evaporation is larger for the Bright Needleleaf simulation, lead-
 286 ing to less latent heat flux (Fig S8b). Despite a higher evaporative resistance, the Needle-
 287 leaf case has the second largest latent heat fluxes ($\sim 46Wm^{-2}$), instead of the Broadleaf
 288 case, as a result of the largest total incoming radiation $\sim 485Wm^{-2}$ (Fig. S8a,b). The
 289 relative amount of sensible heat flux across simulations, which is driven by the gradient
 290 in temperature from the surface to the atmosphere, shows a similar pattern as surface

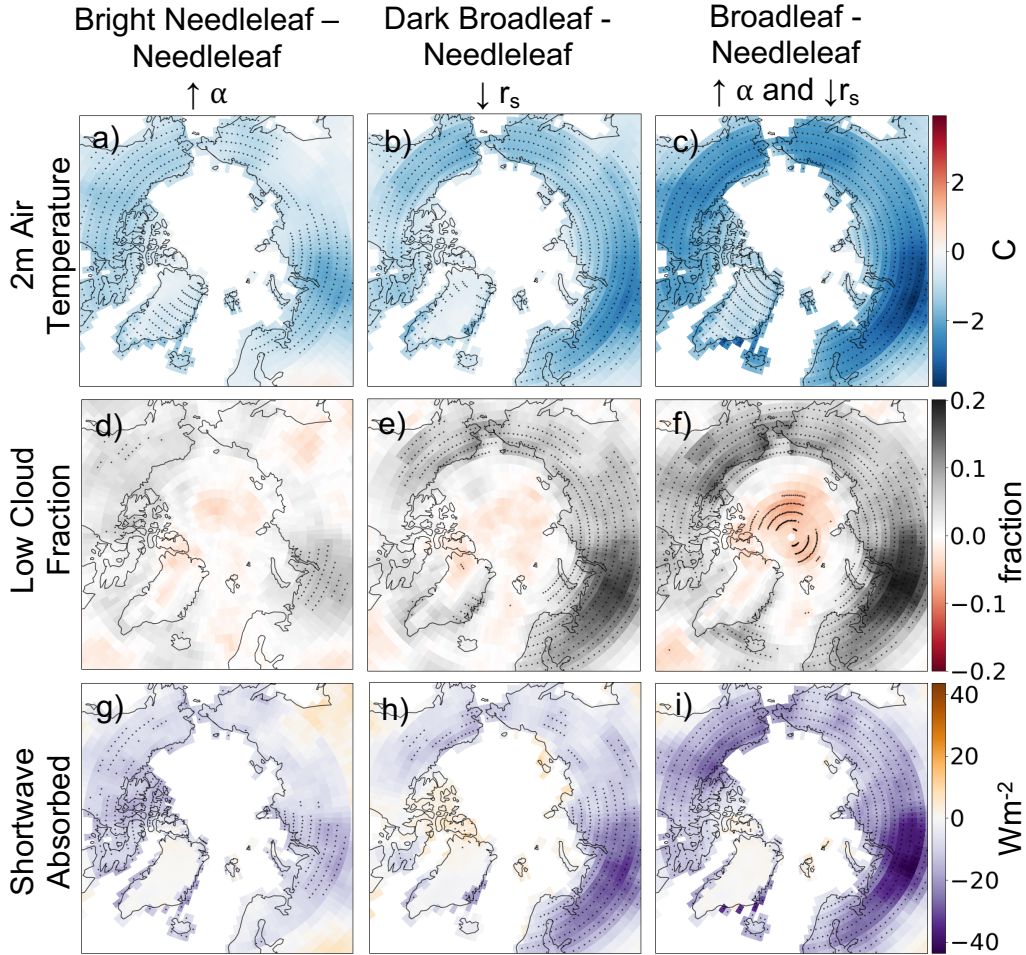


Figure 2. Spatial patterns of change over the Arctic compared to Needleleaf simulation during the summertime. First row (a-c) shows the difference in 2m air temperature (C), the second row (d-f) shows the change in low cloud fraction, the third row (g-i) shows the change in absorbed shortwave radiation (Wm^{-2}) at the surface. Surface temperature and shortwave absorbed are plotted only over land. Column 1 shows the response to increasing albedo (α) alone (Bright Needleleaf - Needleleaf), Column 2 shows the response to decreasing evaporative resistance (r_s) alone (Dark Broadleaf - Needleleaf), and column 3 shows the response to simultaneously increasing albedo and decreasing evaporative resistance (Broadleaf - Needleleaf). Stippling indicates significance.

291 temperature with larger surface temperatures being associated with larger sensible heat
 292 flux, but with a greater distinction between the Bright Needleleaf and the Dark Broadleaf
 293 cases (Fig. S8c).

294 The Needleleaf experiment has the second largest latent heat flux despite having
 295 a high resistance to evaporation. While at first this seems surprising, it can be readily
 296 explained by the fraction of the turbulent fluxes occurring as latent heat flux (LH),
 297 defined as the Evaporative Fraction (EF):

$$EF = \frac{LH}{LH + SH} \quad (3)$$

where SH denotes Sensible Heat fluxes. We find that the low evaporative resistance simulations (Broadleaf and Dark Broadleaf) have relatively higher evaporative fractions of ~ 0.64 compared to the high evaporative resistance simulations (Needleleaf and Bright Needleleaf) which have evaporative fractions of ~ 0.58 (Fig. S8d). The differences in evaporative fraction indicate that simulations with lower evaporative resistance dissipate more energy through latent heat leading to stronger cooling compared with high evaporative resistance simulations regardless of albedo.

Downwelling longwave fluxes emitted by the atmosphere toward the land surface are strongly influenced by surface temperatures (Vargas Zeppetello et al., 2019) and near-surface humidity, and have been observed to be influenced by Arctic cloud cover (Shupe & Intrieri, 2004; Verlinde et al., 2016). In our simulations with warmer surface temperatures, we also find more humid air, and more cloud cover. Thus we expect to see larger downwelling long wave radiation. We find that the greatest downwelling longwave radiation is found in the warmest simulation (Needleleaf with $\sim 330Wm^{-2}$), however the second largest downwelling longwave flux comes from the third warmest experiment (Dark Broadleaf with $\sim 328Wm^{-2}$). Based on surface temperatures alone, we would expect the Bright Needleleaf to have a larger downwelling longwave radiation than the Dark Broadleaf; however, we find that the Dark Broadleaf has more water vapor in the lower parts of the atmosphere and a larger low cloud fraction than the Bright Needleleaf (Fig. 1e, S9c, S10). Thus we hypothesize that the specific humidity and the increase of low clouds may boost the downwelling longwave radiation in the Dark Broadleaf simulation.

3.2 Clouds

The experiments with low evaporative resistance (Broadleaf and Dark Broadleaf) have a greater fraction of low clouds than experiments with high resistance (Needleleaf and Bright Needleleaf), and experiments with low albedos (Needleleaf and Dark Broadleaf) have a smaller fraction of low clouds than experiments with high albedos (Broadleaf and Bright Needleleaf) (Fig. 1e). Given the differences we observe in low cloud fraction across these experiments, we infer that changes in both albedo and evaporative resistance influence cloud formation, although the effect from the change in albedo is not as large as from the change in evaporative resistance. Cloud formation depends on the profile of relative humidity, which in turn depends both on the atmospheric temperatures and specific humidity. Both of these factors may respond to altered surface albedo and evaporative resistance. In particular, albedo and evaporative resistance may influence both the temperature of the atmosphere and the total amount of water vapor, both of which are important for cloud formation. To identify which of these factors is responsible for the change in cloud fraction that we observe in our simulations, we look at the vertical structure of relative humidity, a variable that directly describes how close the air is to saturation. We estimated the contribution to changes in the vertical structure of relative humidity from the changes in the profile of temperature and specific humidity in each of our simulations (using Equations 1&2).

Variations in relative humidity profiles between our experiments are dominated by changes in temperature (Fig. 1f). We find that most of the increase of relative humidity can be attributed to cooling of the vertical temperature profile, driven either by changes in surface albedo or evaporative resistance (Fig. 1f). Compared to the Needleleaf simulation, all other experiments show a decrease in specific humidity, which would also act to reduce the relative humidity (Fig. S10), however, this effect is secondary. We thus find that the increase in relative humidity associated with increasing low cloud cover in our lower evaporative resistance cases (Dark Broadleaf and Broadleaf) is largely driven by cooler temperature profiles in simulations with higher evaporative fraction rather than by direct changes in specific humidity. With cooler temperatures and increased low cloud fraction (Fig. 2a-f), we also find a decrease in the 500 hPa geopotential heights (Fig. S11a-c).

350 Cloud feedbacks occur in response to changes in both albedo and evaporative re-
 351 sistance, resulting in changes to shortwave cloud forcing. Shortwave cloud forcing is de-
 352 fined as

$$SW_{cloud\ forcing} = netSW_{all\ sky} - netSW_{clear\ sky} \quad (4)$$

353 where $netSW_{all\ sky}$ is the shortwave radiation at the top of the atmosphere when the ra-
 354 diative effect of clouds is included (all sky) and $netSW_{clear\ sky}$ is the same but using a
 355 solution from the radiative calculations in the atmospheric model as if there were no clouds
 356 present (clear sky). We find that the simulations with low evaporative resistance (Broadleaf
 357 & Dark Broadleaf) have a greater magnitude of shortwave cloud forcing than the high
 358 evaporative resistance simulations (Needleleaf & Bright Needleleaf), on average by $\sim 9Wm^{-2}$
 359 (Fig. 1d, S6g-i). When evaporative resistance is held fixed and albedo is changed, there
 360 is still a change in shortwave cloud forcing of $\sim 4Wm^{-2}$.

361 Both evaporative resistance and albedo modify shortwave cloud forcing, but through
 362 different processes. Changing evaporative resistance modifies shortwave cloud forcing pri-
 363 marily through the total amount of low cloud cover (Fig. 1c,d), while changing albedo
 364 modifies shortwave cloud forcing through clear sky fluxes of shortwave radiation (Fig.
 365 S7b). Thus, in the case of albedo, even a relatively small change in cloud cover can re-
 366 sult in a substantial change in shortwave cloud forcing because adding clouds above a
 367 dark surface has a greater impact on the amount of SW absorbed by the land surface
 368 than it does over a bright surface.

369 Earlier work by Cho et al. (2018) identified that low cloud feedbacks were an im-
 370 portant factor in determining the surface temperature response to a change in vegeta-
 371 tion cover in the Arctic. However it is unclear from their study how clouds would respond
 372 to a change in evaporative resistance alone. Consistent with Cho et al. (2018), we also
 373 see decreases in low cloud cover and increases in the magnitude of shortwave cloud forc-
 374 ing in response to a darker surface. They propose two possible explanations for the re-
 375 duction in low clouds: first, a reduction in relative humidity caused by an increase in tem-
 376 perature, and second, an increase of roughness causing an increase in the planetary bound-
 377 ary layer height. In our simulations we see large differences in cloud cover and shortwave
 378 cloud forcing due to changes in evaporative resistance which we also attribute to changes
 379 in the vertical profile of temperature; however, in contrast we find a reduction in low cloud
 380 cover and an increase of surface temperature change to be driven by the evaporative frac-
 381 tion rather than the surface roughness. We additionally note that our experimental de-
 382 sign using SLIM allows us to directly separate the effects of surface properties such as
 383 albedo and evaporative resistance on Arctic climate. Future simulations could potentially
 384 be used to isolate the impact of surface aerodynamic roughness, but this is not explored
 385 in this study.

386 3.3 Further Considerations

387 In this paper we have identified that changes in evaporative resistance associated
 388 with a shift in vegetation cover over the Arctic influences the evaporative fraction, re-
 389 sulting in cloud feedbacks which have the same order of magnitude effect on energy fluxes
 390 and surface temperature as changes in surface albedo. This explanation holds in the sum-
 391 mer, but we find that it does not appear in winter due to the accumulated snow cover
 392 and the lack of incoming sunlight, which changes the turbulent fluxes for our simulations.
 393 However, the surface temperature pattern that we see in the summertime in our four ex-
 394 periments appears to persist throughout the year with a smaller magnitude. We hypoth-
 395 esize that the differences in the temperature over land in the wintertime are a result of
 396 differences in the simulated amount of seasonal sea ice (Fig. S12a). The differences in
 397 sea ice in each of the seasons are broadly correlated with the amount of sea ice loss in

398 the summer (Fig. S12b), which we hypothesize to be driven by differences in summer-
399 time temperatures. Thus the differences year-round could be indirectly driven by sum-
400 mertime conditions.

401 We note that actual vegetation has seasonal variations in albedo and evaporative
402 resistance. In this idealized study we have chosen to represent only the summer values
403 of surface properties and are unable to parse the effect of seasonal variations in leaf area
404 by masking snow during shoulder seasons (Cook et al., 2008; Swann et al., 2010; Bon-
405 fils et al., 2012; Luyssaert et al., 2018).

406 Uncertainty in the CLM parameter values used to inform our imposed change in
407 albedo could modify our results. For example, Majasalmi and Bright (2019) find that
408 while CLM has a reasonable representation of visible albedo for boreal plant types, the
409 albedo in the near-infrared is underestimated. A brighter albedo for needleleaf boreal
410 trees in the near-infrared, similar to the near-infrared albedo of broadleaf boreal trees,
411 would reduce the total temperature effect of the change in albedo associated with a change
412 in boreal forest type, although the effect is smaller than it would be for a bias in visi-
413 ble albedos.

414 **4 Conclusions and Implications**

415 We analyzed the effects of specified albedos and evaporative resistances associated
416 with two common tree types in the Arctic: needleleaf evergreen trees and broadleaf de-
417 ciduous trees. We find that evaporative resistance plays a large role in influencing sur-
418 face air temperature over land in the Arctic, similar in magnitude to the influence of sur-
419 face albedo. In simulations with lower evaporative resistance we see that there is an in-
420 crease in the low cloud fraction, which in turn reduces the shortwave radiation incident
421 at the land surface and enhances shortwave cloud forcing. The difference in incident ra-
422 diation due to changes in evaporative resistance is then compounded by changes in albedo
423 in cases where both evaporative resistance and albedo are modified, resulting in dras-
424 tically different temperatures between experiments with differences in both albedo and
425 evaporative resistance (Broadleaf and Needleleaf), and similar temperatures when either
426 one of the surface properties is swapped (Bright Needleleaf and Dark Broadleaf). Our
427 results show that evaporative resistance is as important in influencing Arctic surface tem-
428 peratures as surface albedo and needs to be considered in future studies when trying to
429 understand the effects of vegetation change in the Arctic. These results also demonstrate
430 the usefulness of idealized approaches to land surface modeling (in our case with SLIM)
431 and how we can use this modeling approach to isolate individual surface properties to
432 quantify how changes in specific aspects of the land surface influence the larger climate
433 system. Further studies focused on the role of specific land surface properties and their
434 influence on Arctic climate and circulation could advance our understanding of the po-
435 tential future climate impacts of high-latitude vegetation change.

436 **Acknowledgments**

437 We acknowledge support from the National Science Foundation AGS-1553715 to the Uni-
438 versity of Washington. We would like to acknowledge high-performance computing sup-
439 port from Cheyenne (doi:10.5065/D6RX99HX) provided by NCAR's Computational and
440 Information Systems Laboratory, sponsored by the National Science Foundation. Model
441 results are available through the University of Washington Libraries ResearchWorks dig-
442 ital repository at <http://hdl.handle.net/1773/45281>.

443 **References**

444 Bonan, G. (2015). *Ecological climatology: Concepts and applications* (3rd ed.). Cam-
445 bridge University Press. doi: 10.1017/CBO9781107339200

- 446 Bonan, G. B. (2008). Forests and climate change: Forcings, feedbacks, and the cli-
 447 mate benefits of forests. , *320*(5882), 1444-1449. doi: 10.1126/science.1155121
- 448 Bonan, G. B., Pollard, D., & Thompson, S. L. (1992). Effects of boreal forest vege-
 449 tation on global climate. *Nature*, *359*(6397), 716-718.
- 450 Bonfils, C. J., Phillips, T. J., Lawrence, D. M., Cameron-Smith, P., Riley, W. J.,
 451 & Subin, Z. M. (2012). On the influence of shrub height and expansion
 452 on northern high latitude climate. *Environmental Research Letters*. doi:
 453 10.1088/1748-9326/7/1/015503
- 454 Bretherton, C. S., Widmann, M., Dymnikov, V. P., Wallace, J. M., & Bladé,
 455 I. (1999). The effective number of spatial degrees of freedom of a time-
 456 varying field. *Journal of Climate*. doi: 10.1175/1520-0442(1999)012(1990:
 457 TENOSD)2.0.CO;2
- 458 Chae, Y., Kang, S. M., Jeong, S. J., Kim, B., & Frierson, D. M. (2015). Arctic
 459 greening can cause earlier seasonality of Arctic amplification. *Geophysical Re-
 460 search Letters*. doi: 10.1002/2014GL061841
- 461 Chapin, F. S., Mcguire, A. D., Randerson, J., Pielke, R., Baldocchi, D., Hobbie,
 462 S. E., ... Running, S. W. (2000). Arctic and boreal ecosystems of western
 463 North America as components of the climate system. *Global Change Biology*.
 464 doi: 10.1046/j.1365-2486.2000.06022.x
- 465 Chapin, F. S., Sturm, M., Serreze, M. C., McFadden, J. P., Key, J. R., Lloyd, A. H.,
 466 ... Welker, J. M. (2005). Role of land-surface changes in arctic summer
 467 warming. *Science*. doi: 10.1126/science.1117368
- 468 Cho, M. H., Yang, A. R., Baek, E. H., Kang, S. M., Jeong, S. J., Kim, J. Y., & Kim,
 469 B. M. (2018). Vegetation-cloud feedbacks to future vegetation changes in the
 470 Arctic regions. *Climate Dynamics*. doi: 10.1007/s00382-017-3840-5
- 471 Collins, M., Knutti, R., Arblaster, J., Dufresne, J.-L., Fichet, T., Friedlingstein,
 472 P., ... Wehner, M. (2013). Long-term climate change: Projections, commit-
 473 ments and irreversibility [Book Section]. In T. Stocker et al. (Eds.), *Climate
 474 change 2013: The physical science basis. contribution of working group i to the
 475 fifth assessment report of the intergovernmental panel on climate change* (pp.
 476 1029–1136). Cambridge, United Kingdom and New York, NY, USA: Cam-
 477 bridge University Press. Retrieved from www.climatechange2013.org doi:
 478 10.1017/CBO9781107415324.024
- 479 Cook, B. I., Bonan, G. B., Levis, S., & Epstein, H. E. (2008). Rapid vegetation re-
 480 sponses and feedbacks amplify climate model response to snow cover changes.
 481 *Climate Dynamics*. doi: 10.1007/s00382-007-0296-z
- 482 De Noblet-Ducoudré, N., Boisier, J. P., Pitman, A., Bonan, G. B., Brovkin, V.,
 483 Cruz, F., ... Voltaire, A. (2012). Determining robust impacts of land-use-
 484 induced land cover changes on surface climate over North America and Eura-
 485 sia: Results from the first set of LUCID experiments. *Journal of Climate*. doi:
 486 10.1175/JCLI-D-11-00338.1
- 487 Duveiller, G., Forzieri, G., Robertson, E., Li, W., Georgievski, G., Lawrence, P.,
 488 ... Cescatti, A. (2018). Biophysics and vegetation cover change: A process-
 489 based evaluation framework for confronting land surface models with satellite
 490 observations. *Earth System Science Data*. doi: 10.5194/essd-10-1265-2018
- 491 Edwards, M., Brubaker, L., Lozhkin, A., & Anderson, P. (2005). Structurally novel
 492 biomes: A response to past warming in beringia. *Ecology*, *86*(7), 1696-1703.
- 493 Falloon, P. D., Dankers, R., Betts, R. A., Jones, C. D., Booth, B. B. B., & Lam-
 494 bert, F. H. (2012). Role of vegetation change in future climate under the a1b
 495 scenario and a climate stabilisation scenario, using the hadcm3c earth system
 496 model. *Biogeosciences*, *9*(11), 4739–4756. doi: 10.5194/bg-9-4739-2012
- 497 Foley, J. A., Kutzbach, J., Coe, M. T., & Levis, S. (1994). Feedbacks between cli-
 498 mate and boreal forests during the holocene epoch. *Nature*, *371*(6492), 52-54.
- 499 Gallimore, R., Jacob, R., & Kutzbach, J. (2005). Coupled atmosphere-ocean-
 500 vegetation simulations for modern and mid-Holocene climates: Role of ex-

- 501 tratorial vegetation cover feedbacks. *Climate Dynamics*. doi: 10.1007/
502 s00382-005-0054-z
- 503 Hunke, E., Lipscomb, W., Jones, P., Turner, A., Jeffery, N., & Elliott, S. (2017).
504 *Cice, the los alamos sea ice model, version 00*. Retrieved from [https://](https://www.osti.gov/servlets/purl/1364126)
505 www.osti.gov/servlets/purl/1364126
- 506 Hurrell, J. W., Holland, M. M., Gent, P. R., Ghan, S., Kay, J. E., Kushner, P. J.,
507 ... Marshall, S. (2013). The community earth system model: A framework for
508 collaborative research. *Bulletin of the American Meteorological Society*, *94*(9),
509 1339–1360. Retrieved from <http://dx.doi.org/10.1175/BAMS-D-12-00121.1>
510 doi: 10.1175/BAMS-D-12-00121.1
- 511 Jeong, S. J., Ho, C. H., Park, T. W., Kim, J., & Levis, S. (2011). Impact of veg-
512 etation feedback on the temperature and its diurnal range over the Northern
513 Hemisphere during summer in a 2 CO₂ climate. *Climate Dynamics*. doi:
514 10.1007/s00382-010-0827-x
- 515 Laguë, M. M. L., Bonan, G. B., & Swann, A. L. S. (2019). Separating the impact
516 of individual land surface properties on the terrestrial surface energy bud-
517 get in both the coupled and un-coupled land-atmosphere system. *Journal of*
518 *Climate*.
- 519 Liu, H., Randerson, J., Lindfors, J., & Chapin, F. (2005). Changes in the sur-
520 face energy budget after fire in boreal ecosystems of interior alaska: An an-
521 nual perspective. *Journal of Geophysical Research-Atmospheres*, *110*. doi:
522 ARTND13101
- 523 Lloyd, A. H. (2005). Ecological histories from Alaskan tree lines provide insight into
524 future change. *Ecology*. doi: 10.1890/03-0786
- 525 Luyssaert, S., Marie, G., Valade, A., Chen, Y. Y., Njakou Djomo, S., Ryder, J., ...
526 McGrath, M. J. (2018). *Trade-offs in using European forests to meet climate*
527 *objectives*. doi: 10.1038/s41586-018-0577-1
- 528 Ma, H. Y., Klein, S. A., Xie, S., Zhang, C., Tang, S., Tang, Q., ... Wang, Y. C.
529 (2018). CAUSES: On the Role of Surface Energy Budget Errors to the Warm
530 Surface Air Temperature Error Over the Central United States. *Journal of*
531 *Geophysical Research: Atmospheres*. doi: 10.1002/2017JD027194
- 532 Majasalmi, T., & Bright, R. M. (2019). Evaluation of leaf-level optical proper-
533 ties employed in land surface models. *Geoscientific Model Development*, *12*(9),
534 3923–3938. doi: 10.5194/gmd-2019-59
- 535 Neale, R. B., Gettelman, A., Park, S., Chen, C.-c., Lauritzen, P. H., Williamson,
536 D. L., ... Taylor, M. a. (2012). Description of the NCAR Community Atmo-
537 sphere Model (CAM 5.0). *Ncar/Tn-464+Str*. doi: 10.5065/D6N877R0.
- 538 Royer, D. L., Osborne, C. P., & Beerling, D. J. (2006). Contrasting seasonal pat-
539 terns of carbon gain in evergreen and deciduous trees of ancient polar forests.
540 *Paleobiology*. doi: 10.1666/0094-8373(2005)031(0141:cspsc)2.0.co;2
- 541 Rundqvist, S., Hedenås, H., Sandström, A., Emanuelsson, U., Eriksson, H., Jonas-
542 son, C., & Callaghan, T. V. (2011). *Tree and shrub expansion over the past 34*
543 *years at the tree-line near Abisko, Sweden*. doi: 10.1007/s13280-011-0174-0
- 544 Rupp, T. S., Chapin, F. S., & Starfield, A. M. (2000). Response of subarctic veg-
545 etation to transient climatic change on the Seward Peninsula in north-west
546 Alaska. *Global Change Biology*. doi: 10.1046/j.1365-2486.2000.00337.x
- 547 Schweiger, A. J., & Key, J. R. (1994). Arctic ocean radiative fluxes and cloud forc-
548 ing estimated from the isccp c2 cloud dataset, 1983-1990. *Journal of Applied*
549 *Meteorology*, *33*(8), 948-963.
- 550 Shupe, M. D., & Intrieri, J. M. (2004). Cloud radiative forcing of the Arctic surface:
551 The influence of cloud properties, surface albedo, and solar zenith angle. *Jour-
552 nal of Climate*. doi: 10.1175/1520-0442(2004)017(0616:CRFOTA)2.0.CO;2
- 553 Swann, A. L., Fung, I. Y., Levis, S., Bonan, G. B., & Doney, S. C. (2010). Changes
554 in arctic vegetation amplify high-latitude warming through the greenhouse
555 effect. *Proceedings of the National Academy of Sciences of the United States of*

- 556 *America*, 107(4), 1295-1300. doi: DOI10.1073/pnas.0913846107
557 Thomas, G., & Rowntree, P. R. (1992). The Boreal Forests and Climate. *Quarterly*
558 *Journal of the Royal Meteorological Society*. doi: 10.1002/qj.49711850505
559 Van Cleve, K., Viereck, L. A., Dyrness, C. T., & VanCleve, K. (1996). State factor
560 control of soils and forest succession along the Tanana River in interior Alaska,
561 USA. *Arctic and Alpine Research*.
562 Vargas Zeppetello, L. R., Donohoe, A., & Battisti, D. S. (2019). Does Surface
563 Temperature Respond to or Determine Downwelling Longwave Radiation?
564 *Geophysical Research Letters*. doi: 10.1029/2019GL082220
565 Verlinde, J., Zak, B. D., Shupe, M. D., Ivey, M. D., & Stamnes, K. (2016). The
566 ARM North Slope of Alaska (NSA) Sites. *Meteorological Monographs*. doi: 10
567 .1175/amsmonographs-d-15-0023.1
568 Wolfe, J. A., & Upchurch, G. R. (1987). North American nonmarine climates and
569 vegetation during the Late Cretaceous. *Palaeogeography, Palaeoclimatology,*
570 *Palaeoecology*. doi: 10.1016/0031-0182(87)90040-X